Electron-Positron Annihilation Lifetime Spectroscopy of MgO and Aluminum-Doped MgO

By

Elise D. Liebow

****

Submitted in partial fulfillment

of the requirements for

Honors in the Department of Physics and Astronomy

UNION COLLEGE

June, 2022

ABSTRACT

LIEBOW, ELISE D. Department of Physics and Astronomy, June 2022.

ADVISOR: Dr. Heather C. Watson

Radiation is a form of energy that can damage materials at an atomic level. This has implications for the mobility of radioactive waste through containment materials. We are characterizing atomic defects in materials by using Electron-Positron Annihilation Lifetime Spectroscopy (EPALS). When an electron and positron come into contact with each other, they annihilate and release two antiparallel 511-keV gamma rays. In a pristine crystalline sample, positrons can easily annihilate with electrons, but in a sample with vacancies/defects in the crystal structure, positrons take longer to annihilate. Therefore, the more vacancies in a sample, the longer the average lifetime of a positron in the sample. We measure the lifetime by detecting the time between the emission of a 1274-keV gamma ray when the positron is created and the emission of the 511-keV gamma ray. We have experimentally measured pure, single-crystal MgO samples and found that our results are within the range of past published results (120 ps - 280 ps) with average lifetimes at 258±34.8 ns and 266±12.1 ns. We have also made measurements that span over the course of 1-3 days, resulting in similar lifetimes of 265±2.62 ns. In future experiments, we plan on analyzing pure Fe and Aluminum-doped MgO and then comparing these positron lifetimes with radiation-damaged versions of the same samples.

Contents

1 Introduction

1.1 Radiation Damage and Mitigation

Radiation damages crystal structure of materials at the atomic level. The most significant factor that relates to radioactive damage is the storage of radioactive waste produced at nuclear energy plants. While nuclear energy is a clean source of energy, storing the nuclear waste is a very prominent problem. Nuclear waste can be made up of mostly low-level waste with less than 1% of radiation, but about 3% of the waste contains 95% of all radiation. As seen in Figure 1, nuclear energy is produced when radioactive uranium divides into smaller elements and releases energy. The waste is then cooled in a large pool, then finally sealed in dry cases [1]. The current problem with nuclear energy and its waste is that there is no permanent location to place this radioactive waste without possibly affecting the environment. When radiation leaks into the environment, the long term effects include leakage into nearby bodies of water and living organisms, including plants and animals that live nearby. Radioactive damages in nature have been observed in Chernobyl, Ukraine due to the 1986 Chernobyl accident with a faulty reactor, resulting in two deaths caused by the explosion on site and twenty-eight deaths later from acute radiation damage [2]. Another nuclear plant accident was in Fukushima Daiichi due to a 15-meter high tsunami that disabled three of the four nuclear reactors in 2011 [3]. The main cause for concern when storing radioactive waste is to avoid storing it in a moist or humid area, due to the chance of this radiation-exposed water leaking into the environment and nearby cities.

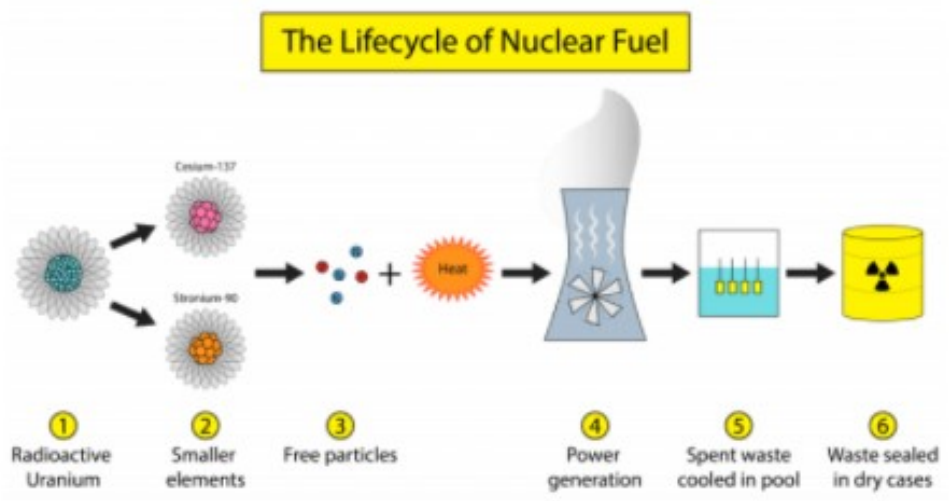

Figure 1: The Life Cycle of Nuclear Fuel. Radioactive Uranium is split into two uneven elements through nuclear fission, which produces free particles and heat, which generates energy in the power generator. The waste products of nuclear fission is cooled in large pools and sealed in dry cases to be stored in salt mines [1].

Scientists now are looking for places to store nuclear waste permanently, which would only be possible if we either find a material that can hold the waste products for thousands of centuries, or to find a sealed underground area that can hold this waste for the same amount of time [1]. Radioactive waste materials are hard to store, but presently are kept at the US Department of Energy: Waste Isolation Pilot Plant (WIPP) in New Mexico, far from any large populations of people [4]. This facility is 26 miles away from the nearest community in Carlsbad, NM and strategically placed away from large bodies of water in the desert. The processing of radioactive waste is handled remotely and transported 2,150 feet underground in ancient salt beds [4]. Remote-handled (RH) radioactive waste is transported in specially designed and tested steel casks that prevent any possible leaks and hold three 55-gallon cylindrical canisters of waste [4]. All nuclear waste that ends up at WIPP must pass all Waste Acceptance Criteria before transported to the disposal location. While this may be a temporary solution, there are still many potential problems that may arise, which can include possible salt bed collapsing and other geological disasters. While this is

a reasonable temporary solution, there have been past accidents that can affect the environment surrounding WIPP. In February of 2014, two unrelated events occurred in the underground portion of the waste plant: a Salt Haul Truck fire and higher readings of airborne radioactivity nine days later [4]. These two accidents did not result in any serious harm, but low levels of radiation were measured in 22 of the 140 workers on site [4].

When creating different ways to store radioactive waste, scientists and engineers want strong material with a limited amount of defects or vacancies within the material. Defects and vacancies are defined as areas where there is a hole or there is a dislocation in crystal lattice of the material, respectively. Radioactive decay produces high energy particles that will travel through the containment material and have the potential to create more defects and damage to the crystal structure. Over a long period of time, this sustained material damage can ultimately lead to failure of the material itself, and radioactive material could leak into the environment. If the radioactive material leaks into the environment, and the groundwater, it could cause widespread harm to nearby life. Most materials that are used for high level radioactive waste containment are metals and ceramics (oxides). Optimizing our methods for containing radioactive waste would also provide more safety for people working close to or near radioactive materials. Moreover, protection from radiation can also be implemented in healthcare, research, and other professions where radiation is a possible risk.

1.2 Calculating Radioactive Decay

Another important way in which radiation is used is through radiometric dating. This technique of measuring the age of metamorphic and igneous rocks, minerals, and meteorites utilizes radioactive isotopes and their half-lives [5]. Due to radioactive decay, the age of a material can be determined by calculating the amount of radioactive isotopes in said material. Radioactivity in a

material has a rate of decay based on the number of atoms (N) in the system, which is:

$$-\frac{dN}{dt} = \lambda N \tag{1}$$

where λ is the decay constant, and the negative sign signifies the rate of decay decreases with time. Once integrated, the resulting equation for radioactive decay is:

$$N = N_0 e^{-\lambda t}. \tag{2}$$

One of the many types of radioactive decay includes beta decay, which depends on the number of neutrons in a system [6]. Since the number of protons determines the element's characteristics, the number of neutrons (can change the stability of an atom). As seen in the equations below, beta decay is the change of a neutron to a proton and a proton to a neutron. Since these transformations can occur, we can change the element by changing the number of protons. The beta particles that are emitted from these subatomic charges are either negatively (electron) or positively (positron) charged, which is based on the starting nucleus. The kinetic energy of the beta particle and the kinetic energy of the antineutrino sum to the total decay energy [6]. Beta particles usually also emit accompanying gamma emissions. The underlying goal in beta decay for a certain isotope is to obtain stability. Too many protons or neutrons makes the nucleus of an atom less stable, creating isotopes that will decay until stability is achieved. Therefore, the starting atom for beta decay happens with an unstable isotope with either more or less neutrons than their usual stable state. The three types of beta decay includes the following:

$$neutron \rightarrow proton + \beta^- + \overline{v} \tag{3}$$

$$proton \rightarrow neutron + \beta^+ + v \tag{4}$$

$$proton + e^{-} \rightarrow neutron + v \tag{5}$$

where the first equation represents neutron decay, the second equation represents proton decay, and the last equation represents when a nucleus captures an extra nuclear electron. Electrons are emitted from a decay of a neutron while a positively charged beta particle is called a positron.

Other types of decay include alpha decay and nuclear fission. Alpha decay is a type of decay that releases an alpha particle, which is made up of two neutrons and two protons and is very similar to a helium, lithium, or beryllium nucleus [6]. This sort of decay happens to nuclei with more than 209 nucleons from the inability to hold all nucleons together from mutual repulsion of the protons and electrons [7]. The alpha particle has a strong bonding energy. Its kinetic energy allows it to escape the nucleus [7]. (Furthermore, alpha particles contain much larger subatomic particles than beta particles), meaning that it is much harder to penetrate certain surfaces with alpha decay than with beta decay. While beta particles must be stopped by thicker materials like sheets of metal or denser material, alpha particles can be stopped by thinner layers of material, like a piece of paper, and do not penetrate the skin when they are close to human contact [8].

The third type of decay is nuclear fission, which is when an unstable nucleus breaks into two different nuclei. This can occur either spontaneously or when certain isotopes of uranium or plutonium absorb neutrons or other subatomic particles [6]. The latter is called induced fission. Since this form of decay produces different, larger atoms, the products are not themselves dangerous, but the copious amounts of gamma rays that result from these radioactive sources are still dangerous as well as the radioactive atoms themselves. Plutonium, a common starting point of nuclear fission, is poisonous and can create a hazardous environment [6].

The main focus in our experiment will be the proton decay, which produces our +positron source for our experiments. Positrons are positively-charged particles created by beta decay.

1.3 Effects of Radiation on Health and Safety

Different types of radiation range from lethal to practically harmless. While any sort of radiation in large amounts is dangerous, gamma radiation is very lethal and can damage living tissue. Beta radiation is much less dangerous, though. This is due to the active site of the radioactive damage of the atom. Gamma radiation is represented by energy waves with a strong penetrative power [9]. When gamma rays are emitted from a radioactive source, they will radiate outwards until they hit another atom, where it can ionize atoms in the body due to the high energy of the radioactive rays. This can alter genetic material and important proteins to everything obstructing the gamma ray's path, making gamma rays extremely lethal. Moreover, gamma radiation is able to pass through the body and cause damage to organic tissues through ionization [10]. Ionization radiation is dangerous to the body due to its ability to break chemical bonds in cells and change charges of atoms. The damage on cells in the body can cause cancer and DNA mutations due to the alterations of certain chemical bonds, like a DNA helix or mutations that can cause uncontrolled growth of cells. To protect oneself from gamma radiation, one would need at least several inches of dense material like lead or steel, since gamma radiation can penetrate concrete to a certain thickness [9].

Beta radiation, on the other hand, is less damaging to living tissue due to their ionization sites. Since beta radiation releases beta particles called positrons, which are antiparticles of electrons, beta radiation only requires a thin sheet of metal in order to protect yourself from beta radiation damage [9]. Beta particles cannot penetrate through the human body, but can penetrate within a few inches into the body. However, when a positron and an electron come into contact, they produce gamma rays, making beta radiation just as dangerous as gamma radiation by itself [11].

Other types of radiation, as mentioned earlier, have different effects on the body. Alpha decay, which emits a small isotope of He, Li, or Be, does not damage the body when the source

is outside the body. This decay can be harmful, but only when ingested [7]. Nuclear fission, on the other hand, is dangerous mainly due to the gamma rays produced by this process. Since this form of decay produces larger atoms, the products are not themselves dangerous, but the gamma rays that result from these radioactive sources are still dangerous as well as the radioactive atoms themselves. Plutonium, a common starting point of nuclear fission, is poisonous and can create a hazardous environment [6]. Therefore, we can see that different types of radiation have varying levels of damage to the materials irradiated.

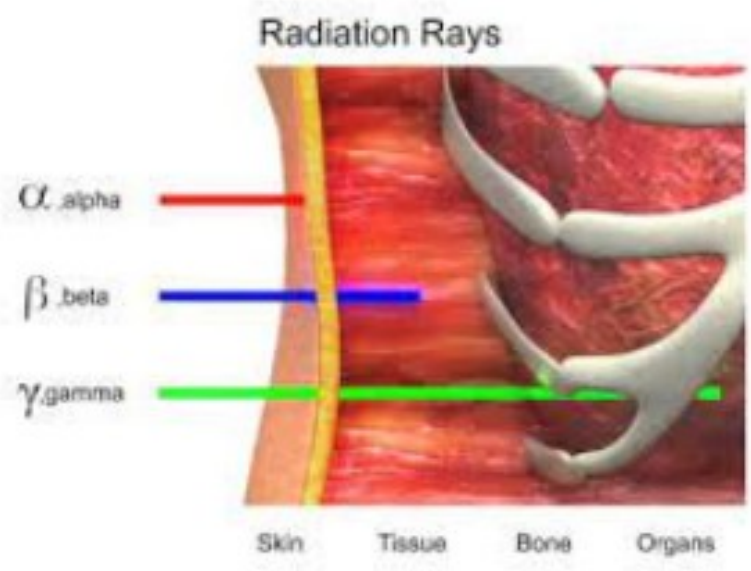

Figure 2: Radiation Affecting the Body. While alpha radiation only affects the dermal layer, beta and gamma radiation enter the body, with gamma radiation completely passing through the body.[8]

1.4 Crystalline Lattices and Imperfections

In this project, we hope to measure and learn more about crystalline defects and vacancies within a crystal structure in a sample of pure MgO. In a crystalline structure, there are many types of defects. A point defect is a defect that only affects a specific point of the material, with limited effect on the rest of the surrounding structure. The most simple point defect is a vacancy, which

is a structure where an atom is missing, also known as the Schottky Effect. The next most simple point defect in a crystalline structure is a substitution impurity, where a new atom replaces the original atom [12]. Other types of point defects include the interstitial impurity, where an extra impurity atom is in between the meeting points of four other atoms, and self-interstitial impurities, which is when an extra atom is placed in the middle of a structured system [12]. There is also the Frenkel defect, which is when a particle is misplaced in the crystal structure, leaving a vacancy and an interstitial insertion. These point defects affect only a small portion of the whole structure, unlike line and plane defects. Other types of defects are based on their effect on the 3-D aspect of the crystalline structure. A line defect affects a row of lattice points and a plane defect affects the entire three dimensional structure of the crystalline material [12]. This can be seen in 3. While these defects are relevant to most crystalline structures, vacancy defects are the most common type of defect in MgO [13].

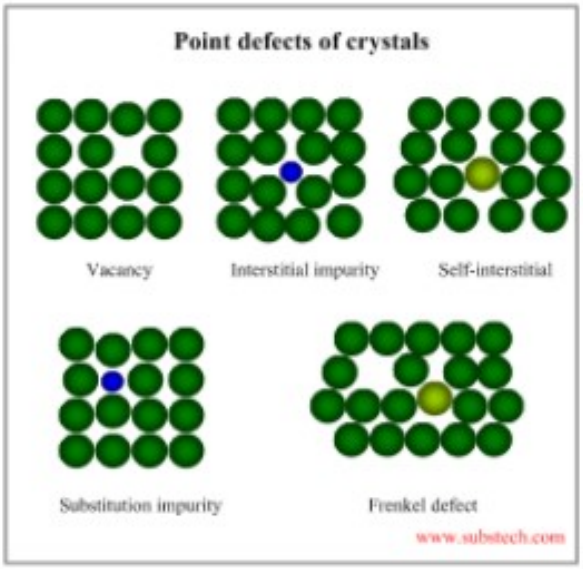

Figure 3: The possible different point defects in a crystal structure. These vary based on the vacancies and possible atomic replacements [12]

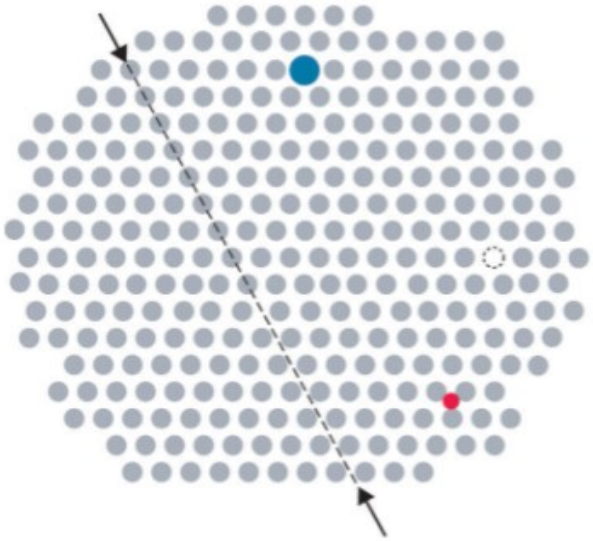

Figure 4: Different vacancies based on their placement in the crystal lattice. The blue, red, and empty spot shows point defects, while the dotted line represents a line defect, where there is a shift at a certain level [14].

The process of doping pure MgO with trivalent cations such as Al3+causes an increase in point defects. These point defects are much more noticeable in doped samples. For instance, our experiment contains pure MgO and aluminum-doped MgO. Since aluminum has a charge of 3+ and magnesium has a charge of 2+, the likelihood of vacancies in the crystalline structure and undergoes a favorable reaction. If an Al3+ atom diffuses into MgO, the substitution will cause a cation vacancy in order to keep the cation balance [13]. Due to the high amount of vacancy defects within MgO, the ability to substitute cations are more abundant than simple Magnesium vacancy defects after diffusion. Moreover, the rate at which cations diffuse is proportional to the number of cation vacancies. Therefore, there can only be a limited amount of Aluminum in the MgO sample.

When using positrons to characterize the number of defects in a sample, the main goal is to understand how electrons are characterized in the space of a crystalline structure. In Figure 3 and 4, the lattice points represent atoms. Therefore, when there is a defect like a vacancy, there is a much smaller chance in finding electrons at that specific location. Since positrons need an electron

in order to annihilate (and release a 511-keV gamma ray that is detected) and that the positron undergoes through a random walk once it enters a solid sample, we can presume that the more defects in a crystalline structure, the longer the positron will last in said sample. This is the main principle of EPALS as discussed in the next section.

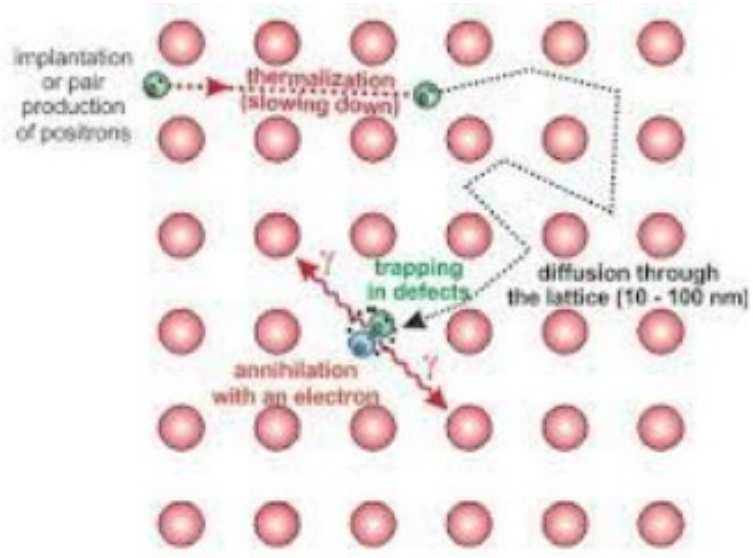

Figure 5: The path of a positron in a crystalline structure. Annihilation occurs when a positron interacts with an electron, but as more vacancies are found in a crystal structure, it is harder for the positron to annihilate with the remaining electrons in the system [15].

1.5 EPALS with MgO and Aluminum-Doped MgO

Electron-Positron Annihilation Lifetime Spectroscopy (EPALS) is a non-destructive form of measuring the relative number of atomic defects and vacancies in a certain material. EPALS uses a radioactive beta source, which emits positrons, the antiparticles of electrons. When an electron and positron come into contact with each other, they annihilate by emitting 511-keV gamma rays. By using beta radiation, we can determine the relative amount of vacancies and defects based on the average lifetime of the positrons emitted from our source. Essentially, the longer the average lifetime of the positron, the more vacancies/defects there are in the material present.

When using positrons to characterize the number of defects in a sample, the main goal is to understand how electrons are characterized in the space of a crystalline structure. In Figure 4 and 5, the lattice points represent atoms. Therefore, when there is a defect like a vacancy, there is a much smaller chance in finding electrons at that specific location. Since positrons need an electron in order to annihilate (and release a 511-keV gamma ray that is detected) and the positron undergoes through a random walk once it enters a solid sample, we can presume that the more defects in a crystalline structure, the longer the positron will last in said sample. This is the main principle of EPALS as discussed in the next section.

In this experiment, we measured positron's lifetimes through a pure MgO sample, and characterize the relative proportion of vacancies through this process. By using EPALS, we also tried to characterize differences between pure MgO and Aluminum-diffused MgO samples, and understand how this process affects the vacancies in the samples. This experiment needs not only the analysis of MgO samples, but also the production and analysis of the aluminum-diffused MgO samples. After observing our pure MgO samples, we measured one experiment of Al-doped MgO to conceptualize the effects of doping pure crystal samples in comparison to future altered samples of MgO.

2 Methods

2.1 Experimental Set-up

The experimental system for EPALS consists of the sample and a beta emitter, the electronic set-up that filters the data, and the computer system that records the filtered data. The first part of EPALS is the radioactive beta source. The beta source emits positrons, which are the main facilitator of this project. 22Na decays into high-energized 22Ne, then releases a 1274 keV gamma ray in order to bring the 22Ne to a ground state, as seen in Figure 6. In our experiments, the detection of the 1274 keV gamma ray signifies the start of the positron's lifetime. Once the positron enters the sample, it then follows a random walk until it reaches an electron, where the positron and electron will then annihilate each other and release two antiparallel 511-keV gamma rays. The detection of the 511-keV rays signifies the end of the positron's lifetime. A timeline of the positron's lifetime is shown in Figure 7.

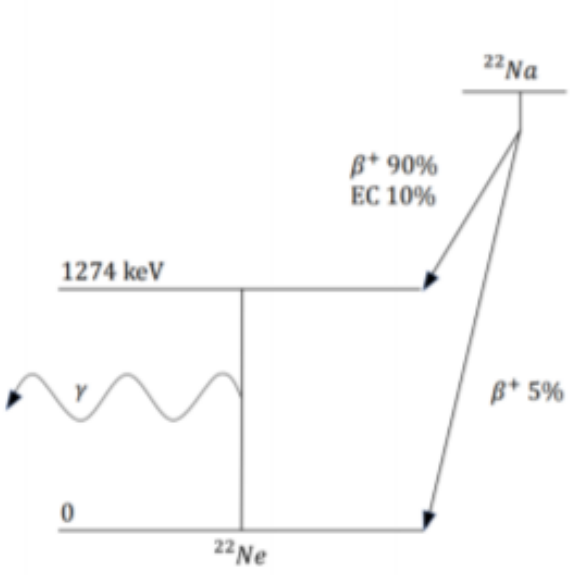

Figure 6: The decay of 22Na from its high energy state. The first step is usually from the 22Na to a high energy 22Ne, which then releases a 1274 keV gamma ray, signifying the birth of a positron [16].

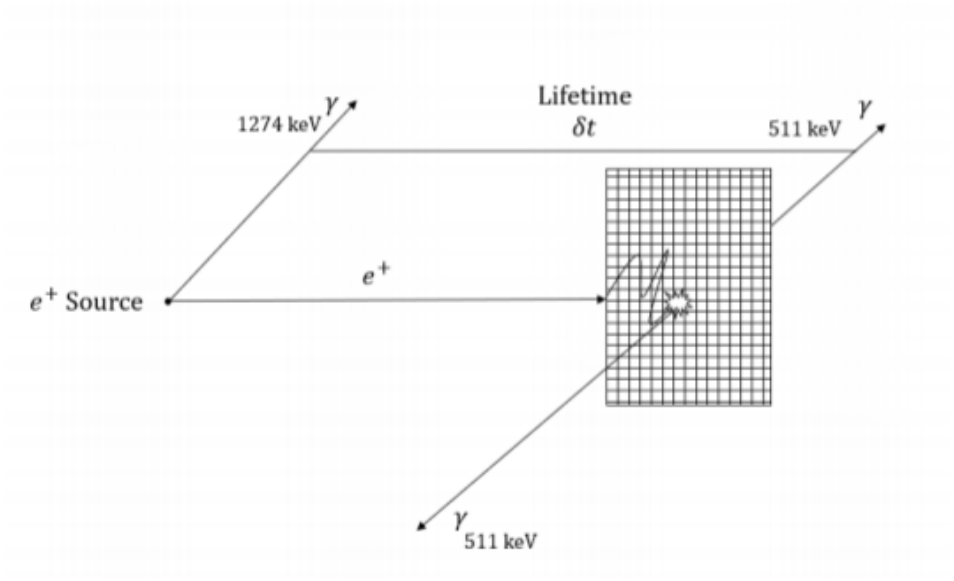

Figure 7: The graphed lifetime of a positron. At the beginning, the 1274 keV gamma ray is released, which is the mark of a positron birth. At the end of its lifetime, the positron comes into contact with an electron, releasing two antiparallel 511 keV gamma rays [17].

In our experimental set-up, the 22Na source is sandwiched between two identical samples of either MgO or Aluminum-doped MgO. The samples are 20 mm x 20 mm x 0.50 mm sheets of single crystal MgO from MSE Supplies, polished on one side. The polished sides are facing each other in the sandwich. This set-up is then placed in between two fast-plastic scintillators that face each other. While one detects the 1274-keV gamma ray, the opposite scintillator measures the 511-keV gamma ray. The set-up can be seen in Figure 8. Each experiment runs for around 16-72 hours. The scintillators are connected to the relevant electronics mentioned in the next section. After connecting the electronics, the computer then collects the data on MAESTRO software. Once the data is collected, we analyze the different lifetimes on the PALSfit3 program made for EPALS measurements. This set-up follows the project by Siegel [17] as well as the ORTEC Experiment 27 [18], which the next section goes more into detail about the connections and electronics behind the experiment. This experiment can also be shown in Figure 9

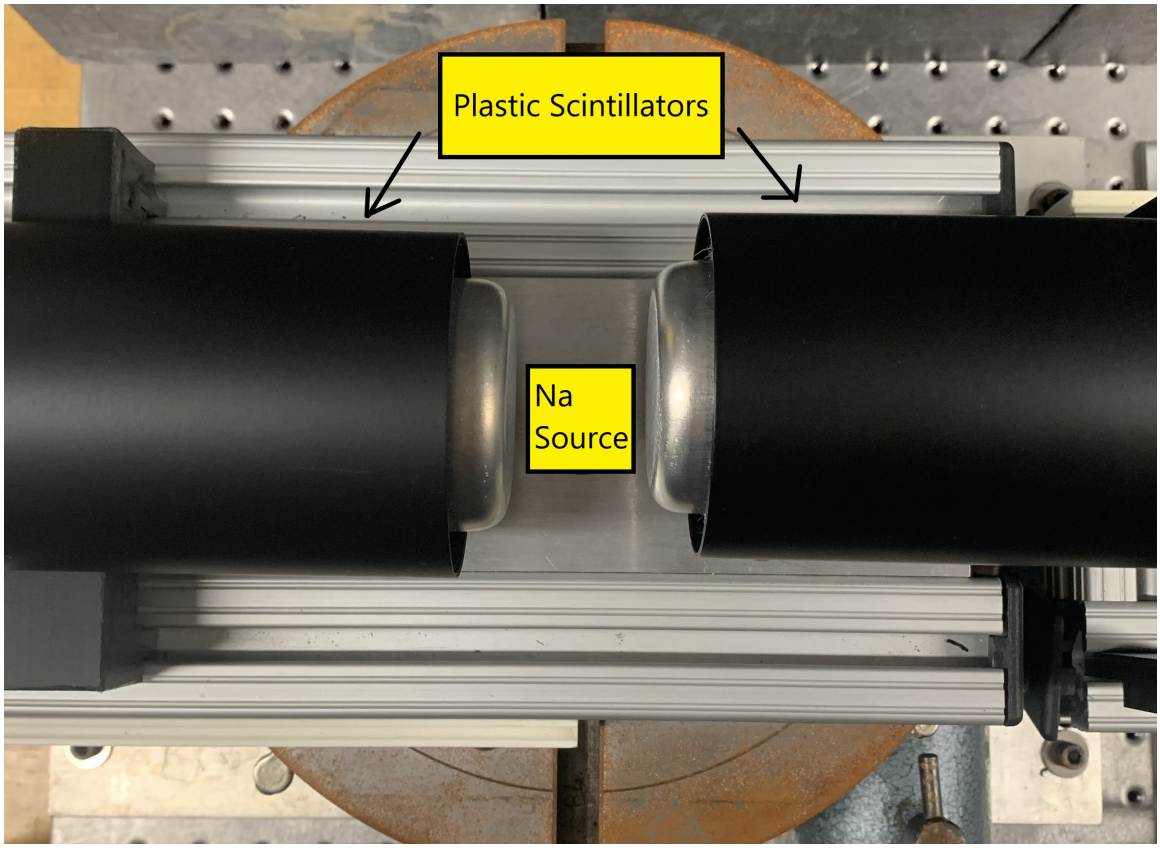

Figure 8: The two plastic scintillators and the placement of the Na Source. One scintillator measures the 1274 keV gamma ray and the other one measures the 511 keV gamma ray, marked as the START and STOP scintillators, respectively.

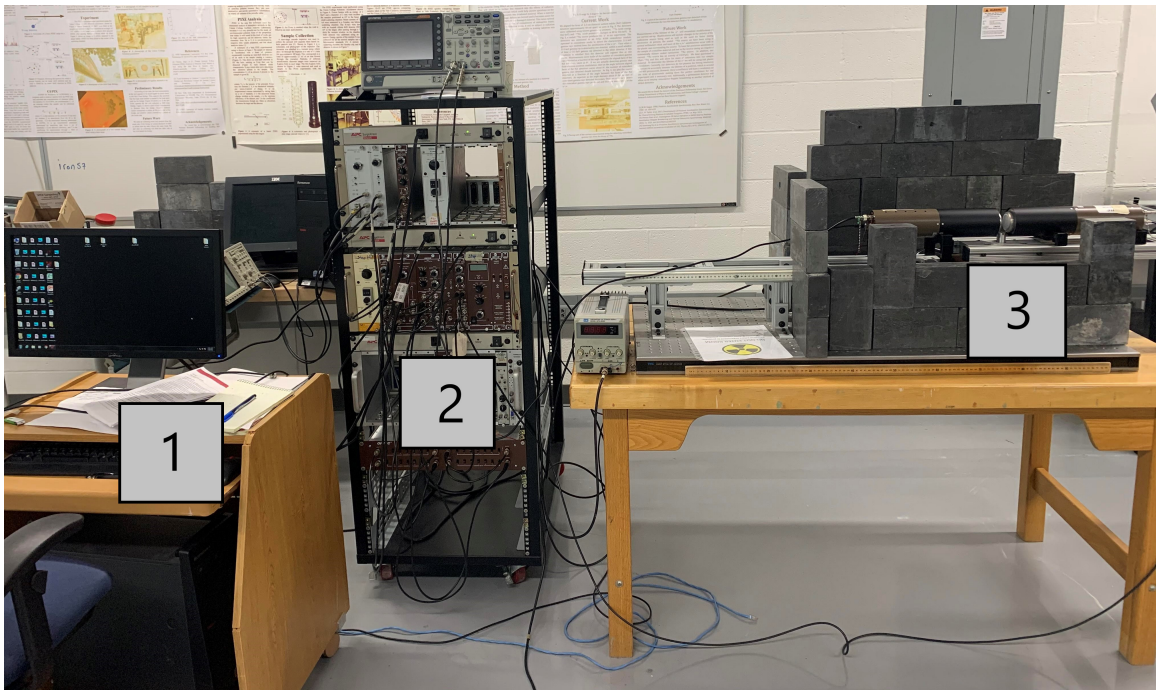

Figure 9: The complete set-up of the experiment, which includes (1) the computer recording the data, (2) the electronic set-up, and (3) the experimental set-up, where the sample and beta source sit.

2.2 Electronic Set-up

The electronics set-up is made up of Figure 10 based on the ORTEC Positron Annihilation Lifetime Spectrometry set-up, also followed by Siegel [17]. The sample and beta source is represented by the black dot in the center, which is surrounded by the two plastic scintillators.

The scintillators connect directly to an R329-02 photomultiplier tube (PMT) and 265A PMT base, where the emitted gamma rays are absorbed into the tube. PMTs are a common tool for spectroscopy that records a given signal into a flashing light when the scintillator detects any form of gamma rays. This makes it possible for the following electronics to identify and record the individual gamma rays produced by the beta source and the positron annihilation. Each of these are powered by a 556 HV Power Supply. The signals from both the START and STOP PMTs

are then sent to the 583B Constant Fraction (CF) Discriminators, each with a 38-cm Delay. The discriminators are there to discriminate between each signal, and the delays are to make sure that correct positrons are relating to each other. The discriminators also clear the irrelevant information when needed. For instance, if a positron's lifetime does not land within a reasonable range, the readings are not recorded. From here, the discriminators lead into ½ DB463 Delay Box to slow down the recording in order for the 567 Time-to-Amplitude Converter (TAC). The 567 TAC is what changes the time readings into a point on a time-by-count graph.

Also coming from the CF Discriminators are the 414A Fast Coincidences. Both discriminators lead into one Fast Coincidence, which checks whether or not each of the readings from both the STOP and START discriminators are correlated. This also leads into the TAC, which then connects finally into the computer to the EASY-MCA 8k MCA System. This final step creates a histogram of all of the readings.

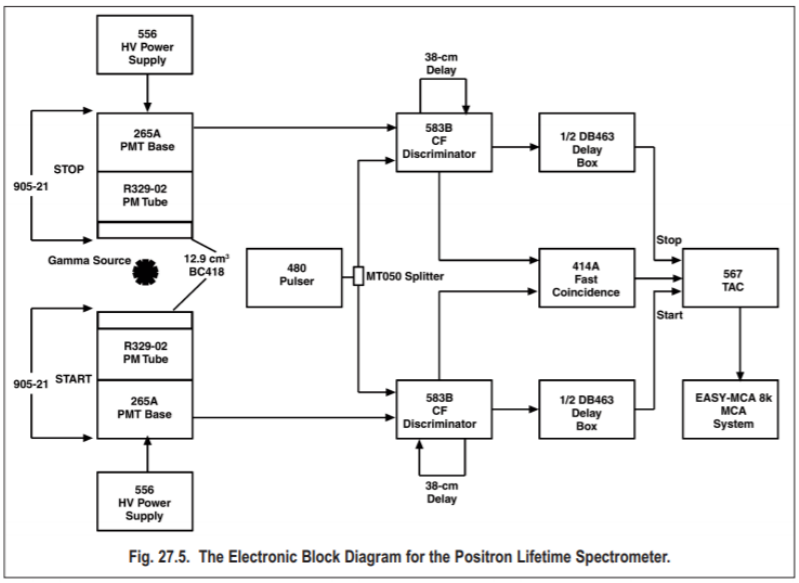

Figure 10: The electronic set-up of the experiment, based on Ortec's Experiment 27: Positron Annihilation Lifetime Spectrometry [18]

2.3 Calibration

In order to calibrate the electronics and scintillators, we used a 480 Pulser and MT050 Splitter to emit controlled, constant pulses for the discriminators to properly measure, as seen in Figure 10. The procedure used to calibrate the system originated from the ORTEC Experiment 27 paper [18]. The beta source was placed between the scintillators, where it would have some sort of positrons to read. The pulser was then set up and connected to both of the CF Discriminators by a MT050 50Ω Matched Tee Signal Splitter. An oscilloscope was connected to the pulser in order to observe the synchronized electronic pulses. We set the pulse height to somewhere between the highest and lowest readings of the CF Discriminators, where we then set the Fast Coincidence reader to connect to the proper channels. When we recorded the results, we set the delays to be 4 ns in order to get a number of readings that were consistent and separated by 4 ns.

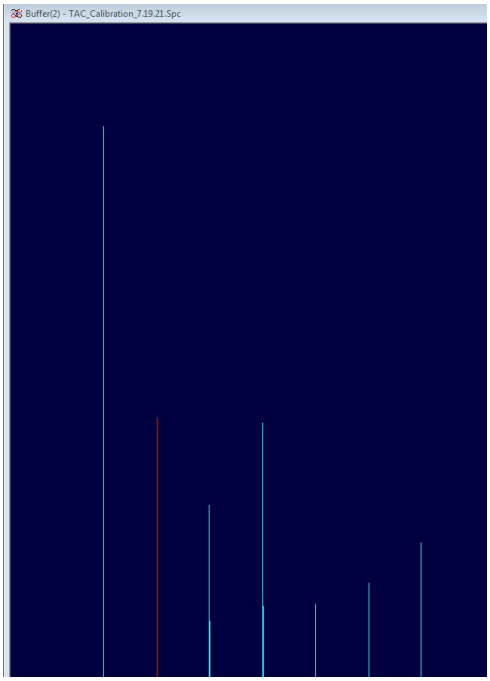

Figure 11: Calibration Graph of the TAC at 4ns from the MAESTRO Program. Each space in between signals represents 4 ns. This chart shows the separation number of channels for every 4 ns with a given signal produced by the pulser. Each peak is produced by the pulser every 4 ns.

Once this was finished, we were able to calculate the separation of channels between each peak positions with the time delays to the time calibration for the spectrometer [18]. The resulting graph is shown in Figure 11, where we find that for every 4 ns, there are 179 channels in between.

2.4 Aluminum Doping for MgO

Our procedure in aluminum-doping our solid MgO sample was based on a paper about aluminum diffusion by Van Orman [13]. Since trivalent cations are easily soluble in MgO and most commonly results in a Schottky defect, the ability to implement Al defects into our samples are possible in high-powered furnaces in the Chemistry Department at Union College [13]. When doping the MgO samples with aluminum, we placed the MgO squares into an aluminum spinel powder and heated the sample to 1075°C for 6 days. This would induce vacancies into our sample by annealing aluminum ions into the crystal structure of our sample. Future experiments will implement longer annealing times and possibly at higher temperatures.

3 Results

3.1 Analysis of Results

In order to analyze our results, we transfer the spectrum from MAESTRO, the recording program we use to collect the data, to another computer where we use the PALSfit3 program. Figure 12 shows the spectrum from the MAESTRO program and Figure 13 shows an example spectrum on the PALSfit3 program, where we analyze the data. Our goal on this program is to get the most accurate reading of our data.

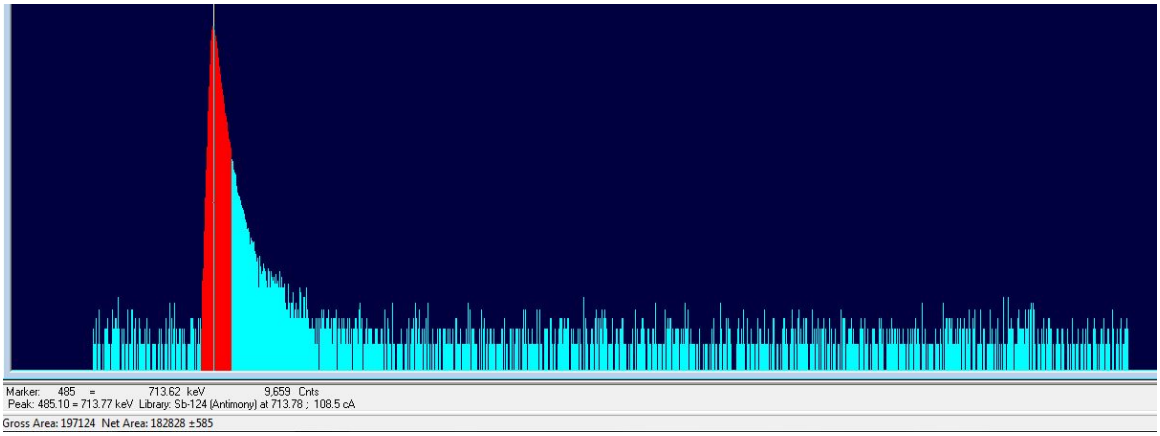

Figure 12: Raw Data from the MAESTRO program of counts of positrons lifetimes. The x-axis represents the lifetime length and the y-axis shows the counts of positrons at lifetime lengths. This is the computer connected to the electronics system that collects the lifetimes in a histogram format.

The different aspects of the program include the resolution fit, the lifetime expected, the second lifetime cycle, and the source correction. The resolution fit correlate with the full widths at half maxima with their relative intensities and their peak intensities (Figure 14)[19]. This is the second tab to the right when analyzing the data. The lifetime expected is in the Lifetimes and Corrections tab and is where we put in our expected lifetime(s) (Figure 15). This places a prediction on where we should see the majority of our lifetimes, based on literature results. In

the same tab, we also can control the second lifetime cycle and the source correction. The second lifetime cycle is to fit the data with the corrected lifetimes found by the source corrections, and the source correction is to consider the other possible materials that might cause the positrons to annihilate prematurely.

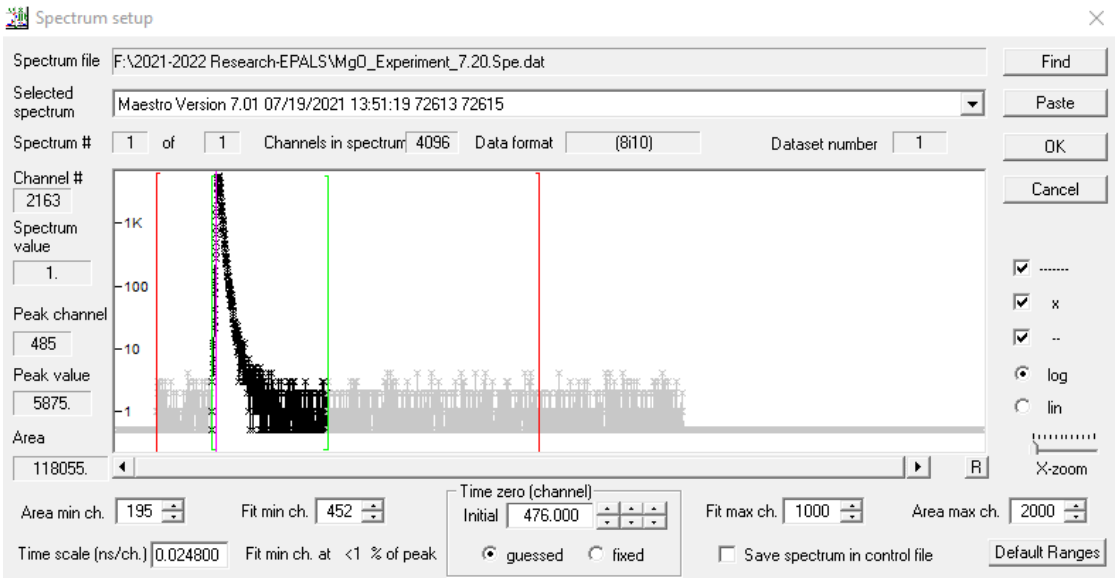

Figure 13: Spectrum setup. This is where we can define what will be read on the PALSfit3 app. The Area min and max channels define the start and end of the total area being observed, and the Fit min and max channels are where the program will fit the curve to. Time zero channel defines where the data will start in reference to fitting the curve. Everything before this will be read and fit, but the final curve will not include anything before the Time zero channel.

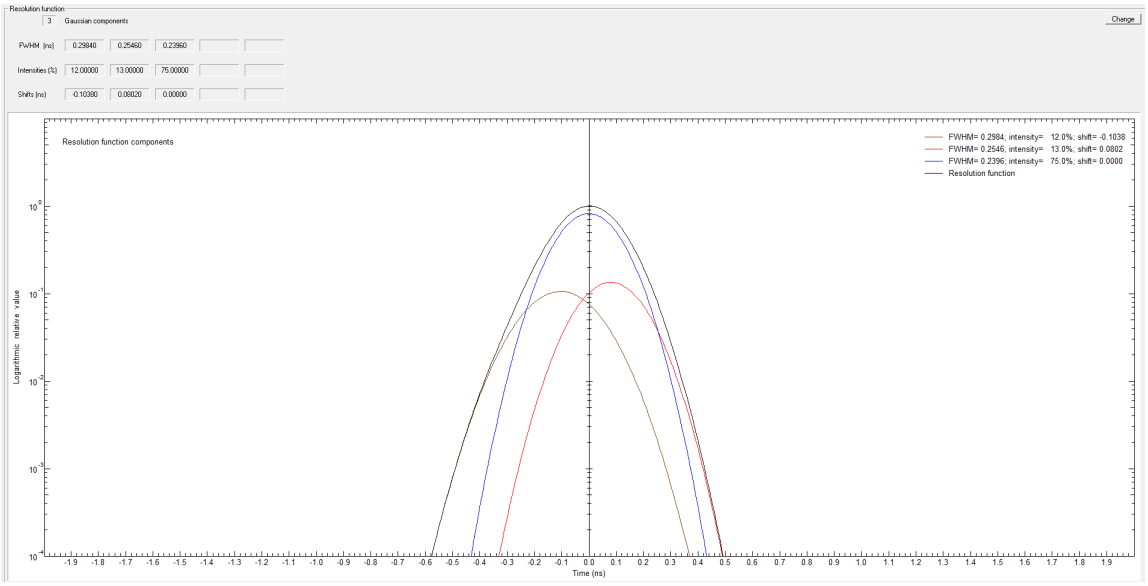

Figure 14: Resolution Fit tab of the PALSfit3 program. This plot is to define the peaks of each lifetime and determine how off-center each peak might be based on the data given.

To create the files, we first worked with what was based on the instruction manual from the PALSfit3 website, which introduces each tab and how changing different aspects of each tab creates a different file to read the experiments [19]. By creating files that were accurate to past MgO standards, we are able to fit each new experiment into said file in order to extrapolate the experimentally measured MgO and Al-doped MgO samples we collect in our project. The original file that we first analyzed was based on the PALSfit3 manual's practice file. These variables and constraints gave us a good starting point to then fill in lifetimes that were more accurate for MgO and that related to the outside constraints. For instance, one of our final files does not have a second lifetime cycle due to the close proximity of the scintillators.

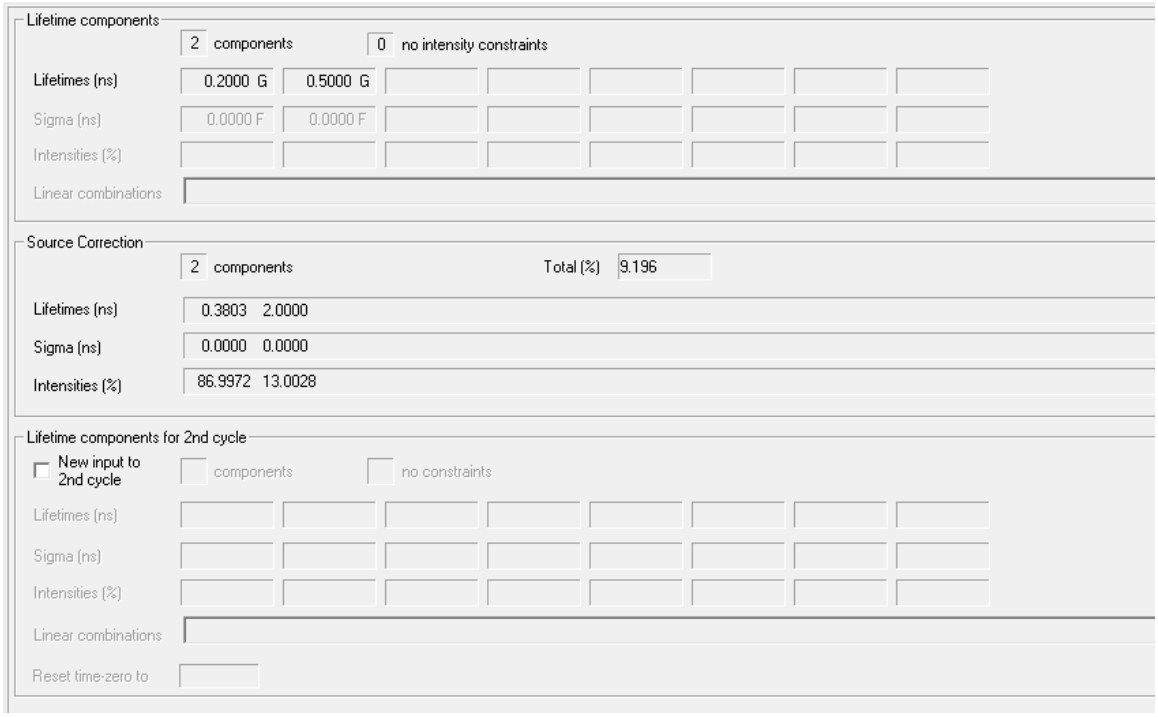

Figure 15: Lifetime and Source Corrections set-up. This function on PALSfit3 lets us estimate the lifetimes measured in a given system as well as possible corrections that might need to be made due to the lifetime of other materials being penetrated by positrons.

In order to make the best-fit files, we adjusted different parameters in order to find a file that best defines all the data collected. We first started with putting in the expected lifetime from literature. A table of file parameters can be references in Appendix A. Our first file was MgOSummer, which was one lifetime at 0.2483 ns. This also had 3 Resolution Functions and has a lifetime 2nd cycle, and was our second most accurate file. The next file made was MgOredo, which had three lifetimes at longer times at 0.2795 ns, 0.5 ns, and 3.2 ns. There is also a lifetime 2nd cycle and three resolution files, but while this file gives precise readings, the readings are larger and therefore not accurate. We then made both of the MgO.better and MgO.betterr files, which each have 1 Resolution function and a Lifetime 2nd cycle, but while the .better file only has a lifetime of 0.2483 ns, the .betterr file has two lifetimes at 0.25 ns and 3.2 ns. Since these files did not give accurate readings, we created a better system, where we first look at the original practice files shown in the PALSfit3 manual, then change the systems based on our experiment. The original practice file

with the same variables as the practice readings was called .FirstStep.Master file, and the second file is called the .2Step.Change. The .FirstStep.Master files has the 3 original Resolution Function, with a 2nd Lifetime Cycle, and the lifetimes of 0.2 ns, 0.5 ns, and 3.2 ns. With reasonable changes in accordance with MgO measurements, we deleted the 2nd Lifetime cycle and the 3.2 ns lifetime in order to make the .2Step.Change file. This file only gave us two expected lifetimes, all of which have reasonable intensities within the range of 0-100, which was not always the case for the past files. All of the other files produced three lifetimes as a result, some of which the intensities were $>100\%$ or $<0\%$. We decided throughout this project that our most accurate files were the MgOSummer file and the .2Step.Change file based on the table in Figure 16.

	Date by Lifetime Chart					
Date of Exp.	MgOSummerOG	_better	_betterr	_FirstStep_Master	_2Step_Change	MgOredo
Date of Exp	MgOSummer File	MgOSummer_better fil	MgOSummer_betterr file	_FirstStep_Master fi	_2Step_Change File	MgOredo file
7.20.21	71.6564/-0.0874	1.6351/-5.9223	0.1252/-1.5245	0.0524/-0.0708	0.1824/68.4916	0.3807/4.3429
	0.2469/100.3497	0.3530/123.6893	0.2524/106.1382	0.2467/100.2830	0.3865/31.5084	0.3806/82.6284
	3.6030/-0.2623	0.6714/-17.7670	1.0021/-4.6036	5.4004/-0.2123		2.0008/13.0287
mean	0.1756	0.2206	0.2198	0.2359	0.2467	0.5917
7.23.21	0.0925/86.4092	81.2132/-0.2297	70.1036/-0.2204	66.5616/-0.0298	0.2073/80.9357	1.3168/0.2122
	0.1987/-245.6368	0.2421/100.9115	0.2409/100.8817	0.2530/100.1193	0.4701/19.0643	0.2941/99.1513
	9999.9999/259.2276	1.5620/-0.6836	1.6093/-0.6613	6.1774/-0.0894		1.6620/0.6365
mean	9999.9999	0.0486	0.0779	0.2279	0.2574	0.305
7.26.21	0.2617/2.2990	0.0494/1.8535	0.0500/2.0483	0.6676/1.7189	0.2616/93.1225	0.3268/0.2043
	0.2617/90.8041	0.2532/92.5859	0.2516/91.8066	0.2616/93.1245	0.6677/6.8775	0.3178/99.1827
	0.6697/6.8969	0.6569/5.5606	0.6390/6.1450	0.6674/5.1566		2.1931/0.6130
mean	0.2898	0.2719	0.2713	0.2895	0.2895	0.3293
7.27.21	0.9103/2.5114	0.0386/0.0924	0.3342/0.0739	0.0000/1.4084	0.2355/88.1868	0.0092/-12.9561
	0.2434/89.9543	0.2555/99.6305	0.2550/99.7044	0.2542/94.3664	0.5919/11.8132	0.2765/151.8242
	0.4839/7.5343	1.8093/0.2772	1.9474/0.2217	0.7983/4.2252		0.2765/-38.8682
mean	0.2783	0.2596	0.2588	0.2736	0.2776	0.3112
7.28.21	1.0331/0.1345	0.0008/-2.7550	335.3008/-4.6326	0.0311/0.4216	0.2008/75.3208	0.3061/0.3550
	0.2574/99.4620	0.2862/111.0202	0.3197/118.5305	0.2537/98.3136	0.4537/24.6792	0.3009/98.5802
	1.4172/0.4035	0.8529/-8.2651	0.8722/-13.8978	0.9599/1.248		1.7904/1.0649
mean	0.2631	0.2472	-15.2755	0.2617	0.2632	0.3168
11.2.21	0.0000/0.1012	8.5807/0.0166	0.1303/-3.4424	0.0000/0.1022	0.2097/78.8886	0.3809/4.3536
	0.2570/99.5951	0.2427/99.9335	0.2886/113.7694	0.2564/99.5911	0.4552/21.1114	0.3809/82.5858
	1.9702/0.3036	8.5282/0.0498	0.8261/-10.3271	1.8633/0.3067		2.0008/13.0607
mean	0.2619	0.2482	0.2385	0.261	0.2615	0.5925
11.3.21	1.0918/0.1111	7.8061/0.0120	0.8099/-18.6187	0.0197/2.6962	0.2154/82.8978	0.3814/4.3623
	0.2583/99.5556	0.2450/99.9520	0.3055/174.4748	0.2355/89.2153	0.5065/17.1022	0.3814/82.5510
	2.0336/0.3333	7.8673/0.0360	3832.0336/-55.8561	0.6119/8.0885		2.0019/13.0868
mean	0.2651	0.2487	-2140.041	0.2601	0.2652	0.5935
11.5.21	0.0265/0.3831	0.8836/-29.3277	4.5457/0.0121	1.4845/0.3697	0.2119/80.7118	0.3832/4.4252
	0.2559/98.4674	0.3374/217.3110	0.2451/99.9517	0.2539/98.5210	0.4898/19.2882	0.3832/82.2993
	1.1659/1.1494	2738.4421/-87.9832	4.5660/0.0362	0.8779/1.1092		2.0028/13.2755
mean	0.2655	-2408.8961	0.2471	0.2653	0.2655	0.5982
11.8.21	0.0304/0.5680	4.5771/0.0240	0.9384/-34.4167	0.0305/0.6062	0.2171/83.3598	0.3838/4.4219
	0.2556/97.7582	0.2479/99.9040	0.3568/237.6669	0.2546/97.5752	0.5281/16.6402	0.3838/82.3125
	1.0763/1.7039	4.4836/0.0720	2161.6284/-103.2502	1.0362/1.8186		2.0041/13.2656
mean	0.2683	0.252	-2231.3608	0.2674	0.2689	0.5987

Figure 16: Files and Lifetimes with Related Intensities, organized by lifetime in ps/intensity of lifetime. We can notice the most amount of intensities under 100 in the MgOSummer file and the .2Step.Change file, showing that these are the most accurate files for reading the data measured.

With these two files, we were able to fit the rest of our data with both pure MgO experiments and Al-doped MgO experiments, resulting in lifetime spectra like Figure 17.

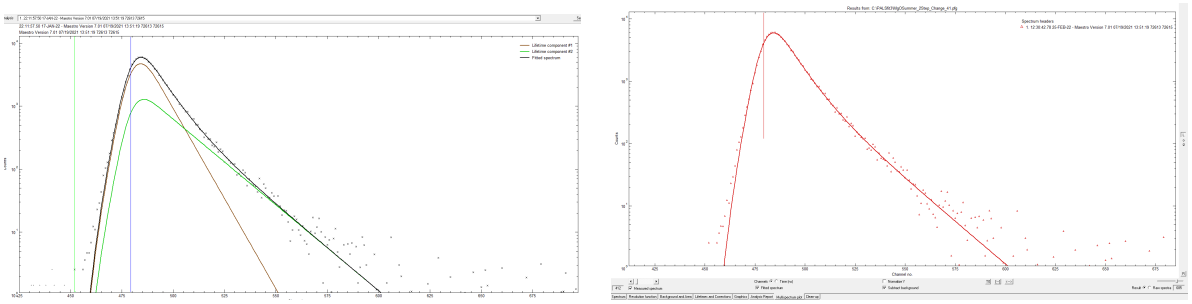

Figure 17: a) the resulting Lifetime plots and b) the resulting Multispectrum Plot. The multispectrum plot is made up of the average of the lifetime plots to get one defining spectrum to characterize the average lifetime.

3.2 Pure MgO

The Pure MgO experiments tested both the positron lifetimes and differing length of time for experiments. These two factors were tested separately during the summer of 2021 and November 2021, respectively. The first five experiments from July ran at similar times, for about 1-2 days, whereas the experiments in November measured the lifetimes of the positrons at varying lengths of time, ranging from 1-4 days. The parameters for each experiment can be seen in Appendix B. The results for all nine experiments showed many similarities in experimental lifetimes measured. For instance, the results from different lengths of time measured similar lifetimes, which shows that the length of experiment does not affect the results.

The most prominent lifetimes ranged from 255±6.15 ps in our pure MgO samples based on our MgOSummer file, and 216±22.2 ps from the .2Step.Change file. The uncertainty is based on the standard deviation of the resulting lifetimes calculated by Excel standard deviation function. The average lifetimes based on the MgOSummer file was 258±34.8 ps. Likewise, the average lifetime for the .2Step.Change file is 266±12.1 ps. Most of our results for both files fell within the range of 260-290 ps, displaying a consistency with lifetimes throughout many experiments. Our

Exp. Date	Collection Time	MgO.Summer Most Intense	MgO.Summer Mean Lifetime	2Step.Change Most Intense	2Step.Change Mean Lifetime
7.20.21	NM	0.2469	0.1756	0.1824	0.2467
7.23.21	19h 28m	NA	NA	0.2073	0.2574
7.26.21	17h 34m	0.2617	0.2898	0.2616	0.2895
7.27.21	20h 37m	0.2434	0.2783	0.2355	0.2776
7.28.21	21h 18m	0.2574	0.2631	0.2008	0.2632
11.2.21	24h 10m	0.2570	0.2619	0.2097	0.2615
11.3.21	24h	0.2583	0.2651	.2154	0.2652
11.5.21	48h	0.2559	0.2655	0.2119	0.2655
11.8.21	71h 56m	0.2556	0.2683	0.2171	0.2689
AVGS		0.254525	0.25845	0.215744444	0.266166667
STAND DEV		0.006153686	0.034775689	0.02222831	0.012095454

Table 1: Final Observable Results of the MgO.Summer File and 2Step.Change file. The most intense lifetimes are the lifetimes that dominated the majority of the mean lifetime.

complete table of experiments can be found in Table 1.

3.3 Al-Doped MgO

The results from the Al-doped MgO have shown very little difference in what was measured in the Pure MgO, which can be expected at certain levels of annealing to the Al spinel. Our longest duration of submerging the MgO samples in the Al spinel was for six days at 1075°C. The average resulting lifetime and most prominent from the MgOSummer file were 266±12 ps and 251±88 ps, respectively. The average and most prominent lifetimes from the .2Step.Change file are 267±12.1 ps and 218±12.1 ps, seen with resulting lifetime spectra in Figure 18.

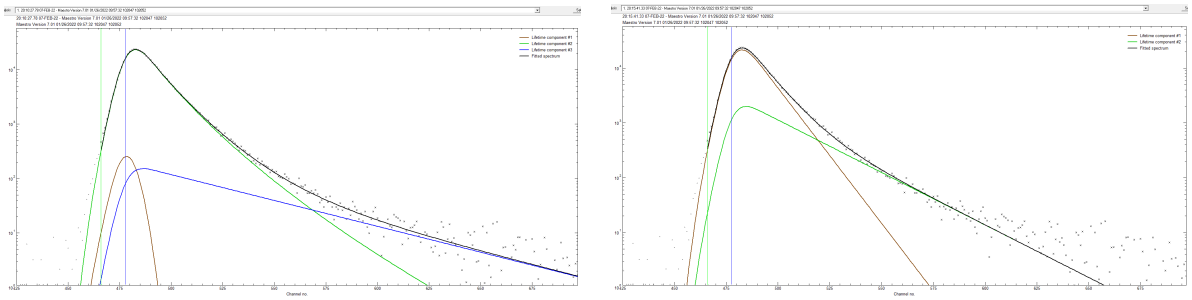

Figure 18: The lifetime spectra of a) MgO.Summer file and b) 2Step.Change file for AL-doped MgO. The black line for both spectra are the average lifetimes measured, whereas the colorful lifetimes are the different lifetimes components.

4 Discussion and Conclusion

The results we measured show the lifetime a positron lasts inside a pure MgO crystal. The most prominent results are the positron's most characteristic lifetimes, as shown in Figures 17 and 18. These lifetimes characterize the majority of the lifetimes, but not the entire average lifetime The average lifetime consists of all of the measured lifetimes. While these two lifetimes are usually close in value, that is not always the case. According to our results, the most prominent lifetimes were lower than the average lifetimes, meaning that there were lifetimes that were longer than the most prominent lifetime. This conclusion can represent possible vacancies in the crystal structure, which would be characteristic of a realistic 'pure' sample of an MgO crystal. This could be due to the inability to have a perfectly pure crystal structure due to manufacturing procedures or natural sources of decay.

Our results align very well with past results and show promising similarities. A range of lifetimes with varying intensities are generally the results of an EPALS experiment, with one or two lifetime(s) that usually dominate the overall lifetimes. This characterizes the majority of the mean lifetime. The lifetimes of previous papers confirm lifetimes that dominate mainly in the range of 237.0-291.0 ps with annealed MgO at different temperatures between 600-1000K [20]. More research shows that there are also lifetimes in the shorter range, from 121-178 ps, detailing that there are a range of multiple lifetimes that also represents shorter lifetimes [21][22][23]. These shorter lifetimes include lifetimes of 145.5 ps for 45.6% of the lifetimes at 800K annealing temperature, and 115.9 ps for 30.9% of the lifetimes at annealing temperature 1000K [20]. While these lifetimes do not correspond to our data, more analysis can be done to continue to understand vacancies of MgO. The lifetimes from the insulator model in the Mizuno paper were between 121-180 ps, which are too short to correspond to the results that we obtained, but the semiconductor model fits our data more in the range of 131-201 ps [21]. The experimental results from this paper are in the range of 130-185 ps, just outside the range of our results. The Das et. al. paper shows a range of lifetimes from 153-400 ps, which would confirm our experimental results [23]. Moreover,

while the lifetimes measured by Mizuno et. al. do not agree with our results, we do see an increase in lifetime when doping the MgO crystal with other trivalent atoms [22]. The calculated lifetimes from past papers do not align perfectly with our results, showing that our analysis method could be off [20][21].

The lifetimes found are reasonably longer than 0 ps due to the time it takes for the positron to enter the sample and come into contact with an electron. A major difference between many of the experiments was that some past papers used a powdered version of MgO instead of a sample of solid MgO that we used [23][20]. Moreover, the calculations from the Mizuno paper [21] reports that there are two ways to look at MgO: as an insulator and as a semiconductor, due to its different properties of both atoms in the crystal. These calculations can cause a difference in the freedom of electrons in the system, since electrons can move more freely in a semiconductor model than for an insulator system, which is evident in the movement of electrons in conductors and semiconductors [24]. Since insulators have a much more rigid structure in electron movement, we notice that the calculated lifetime for insulators are longer than those for semiconductors, which illustrates the partial freedom of electrons in the latter system than the former. Consequently, the lifetime for an insulator model would be 167 ps, while for a semiconductor model, it had a calculated lifetime of 119 ps [25]. These are one of many things to consider when calculating the lifetime for MgO.

Moreover, the results gained from the Al-doped MgO are significant to our understanding of how radiation affects single-crystal structures. By increasing the amount of Aluminum in our MgO crystal, we can model how radiation can affect an impure sample with more vacancies and defects. By using EPALS, the vacancies can be measured for these impurities, which gives us a better understanding of how radiation affects the crystal structure of materials. Since we were only able to run one experiment in two terms, we are not able to draw any conclusions from our results, but plan on running more experiments on these samples at different lengths of time for annealing the aluminum in the near future.

Many other experiments have been proposed in order to gain a better grasp on how radioac-

tivity affects crystal structures. While pure Fe samples are a common option for running EPALS experiments, we also have some samples of Argon-doped crystal structures. These samples were infused with Argon via an Ar ion beam at the University of Albany. Furthermore, we plan on looking at samples of MgO that have been irradiated for different amounts of time, which can help us conceptualize the crystal structure of irradiated samples and their vacancies that result from radiation.

In this thesis project, we were able to measure the lifetime of positrons in pure crystalline MgO samples at different lengths of time in order to characterize the amount of vacancies in a standard MgO crystal. We created multiple files that could correctly analyze and extrapolate the average positron lifetime in a sample and provide major and minor lifetimes to describe the average lifetime on PALSfit3. Finally, we measured and analyzed the average and most intense lifetimes for an Aluminum-doped MgO crystal. Moreover, possible analysis methods to characterize vacancies in the future can include using atomic force microscopy, X-ray diffraction, or an atomic microscope. Both would give us a better understanding of the vacancies within our specific samples. (Some further experiments that we hope to continue in the future are more measurements for Aluminum-doped MgO samples at different annealing times, irradiated samples of MgO, pure Fe samples, and irradiated samples of Fe.)ENG These measurements will provide a baseline understanding of how irradiated materials can have more defects in their molecular structure than a pure crystal structure.

References

[1] M. Jennewein and R. Senft, *Looking for a trash can: Nuclear waste management in the united states*, 2018. [Online]. Available: https://sitn.hms.harvard.edu/flash/2018/looking-trash-can-nuclear-waste-management-united-states/.

[2] *Chernobyl — chernobyl accident*, 2022.

[3] *Fukushima daiichi accident*, Apr. 2021. [Online]. Available: https://world-nuclear.org/information-library/safety-and-security/safety-of-plants/fukushima-daiichi-accident.aspx.

[4] U. D. of Energy, *Waste isolation pilot plant*, 2021. [Online]. Available: https://www.wipp.energy.gov/.

[5] I. Graham, *Radioactive dating*, Sep. 2020. [Online]. Available: https://australian.museum/learn/minerals/shaping-earth/radioactive-dating/.

[6] G. Faure, *Principles and applications of geochemistry*, 2nd. Prentice Hall Upper Saddle River, NJ, 1997, vol. 625, pp. 276–284.

[7] A. Beiser, *Concepts of Modern Physics (SIE)*. McGraw-Hill Education, 1963.

[8] *Radiation rays: Alpha, beta, and gamma*, Jun. 2015.

[9] EPA, *Radiation protection: Radiation basics*. [Online]. Available: https://www.epa.gov/radiation/radiation-basics.

[10] L. Gilstrap, *Radiation and cancer*, Nov. 2016. [Online]. Available: https://serc.carleton.edu/NAGTWorkshops/health/case_studies/radiation_cance.html.

[11] J. Kuriplach, "Calculation of positron response from embedded nanoparticles," *Acta Physica Polonica A*, vol. 107, no. 5, pp. 784–791, 2005.

[12] D. Kopeliovich, *Imperfections of crystal structure*, Jun. 2012. [Online]. Available: https://www.substech.com/dokuwiki/doku.php?id=imperfections_of_crystal_structure.

[13] J. V. O. A., C. Li, and K. L. Crispin, *Aluminum diffusion and al-vacancy association in periclase*, ID: ctx3987934420004651, 2009. DOI: 10.1016/j.pepi.2008.03.008.

[14] A. Schmitz, *General Chemistry: Principle, Patterns, and Applications*, 1st ed. Saylor Academy, 2012.

[15] M. Butterling, *Positron annihilation*. [Online]. Available: https://www.hzdr.de/db/Cms?pOid=35245&pNid=3225.

[16] J. Feinstein, "Electron positron annihilation lifetime spectroscopy/an introduction for union college," 2021.

[17] R. W. Siegel, "Positron annihilation spectroscopy," *Annual Review of Materials Science*, vol. 10, no. 1, pp. 393–425, 1980.

[18] ORTEC, "Experiment 27: Positron annihilation lifetime spectroscopy," Tech. Rep.

[19] P. Kirkegaard, J. V. Olsen, and M. M. Eldrup, "Palsfit3: A software package for analysing positron lifetime spectra," Technical University of Denmark, Tech. Rep., Jun. 2020.

[20] N. Pathak, S. K. Gupta, C. L. Prajapat, *et al.*, "Defect induced ferromagnetism in mgo and its exceptional enhancement upon thermal annealing: A case of transformation of various defect states," *Physical Chemistry Chemical Physics*, vol. 19, no. 19, pp. 11 975–11 989, 2017.

[21] M. Mizuno, H. Araki, and Y. Shirai, "Theoretical calculations of positron lifetimes for metal oxides," *Materials transactions*, vol. 45, no. 7, pp. 1964–1967, 2004.

[22] M. Mizuno, Y. Inoue, K. Sugita, *et al.*, "Positron annihilation study of formation of mg vacancy in mgo," in *Materials Science Forum*, vol. 445, Trans Tech Publ, 2004, pp. 153–155.

[23] A. Das, A. C. Mandal, S. Roy, *et al.*, "Synthesis and characterization of magnesium oxide nanocrystallites and probing the vacancy-type defects through positron annihilation studies," *Physica E: Low-dimensional Systems and Nanostructures*, vol. 83, pp. 389–397, 2016.

[24] M. J. Puska and R. M. Nieminen, "Defect spectroscopy with positrons: A general calculational method," *Journal of Physics F: Metal Physics*, vol. 13, no. 2, p. 333, 1983.

[25] M. J. Puska, S. Mäkinen, M. Manninen, and R. M. Nieminen, "Screening of positrons in semiconductors and insulators," *Physical Review B*, vol. 39, no. 11, p. 7666, 1989.

Appendices

Appendix A File Parameters

Here are the parameters for each file from the Results section:

File Name	Lifetimes	Lifetime 2nd cycle	Resolution Function
MgOSummerOG	0.2483	Y	3
_better	0.2483	Y	1
_betterr	0.25 3.2	Y	1
_FirstStep_Master	0.2 0.5 3.2	Y	3
_2Step_Change	0.2 0.5	N	3
MgOredo	0.2795 0.5 3.2	Y	3

Appendix B Standards for Experiments

Unchanged Parameters for all exp: Counter time calibrated

Min Pulse Height for STOP: 1.75 with 2 attenuator, switched to 7.40

Min Pulse Height for START: 1.64

No Change of Delays

Unchanged Parameters: CF Discriminator Measurements:

Start: Upper: 378 Lower: 182

Stop: Upper: 242 Lower: 26

Date	Length of Time	Counts	Distance of Scintillators
7.20.21	UNKNOWN, about 17hr	118,518	UNKNOWN
7.23.21	19h28m	110,254	4.6 cm
7.26.21	17hr34m	52,886	4.5 cm
7.27.21	20hr37m	196,326	4.4 cm
7.28.21	21hr18m	243,620	4.4 cm
11.2.21	24hr10m	204,921	4.0 cm
11.3.21	24hr	236,656	4.0 cm
11.5.21	48hr	583,738	4.0 cm
11.8.21	71hr56m	1,161,930	4.0 cm